Enhanced Cytosolic Delivery and Releases of CRISPR/Cas9 by Black Phosphorus Nanosheets for Genome Editing

Wenhua Zhou,[+a] Haodong Cui,[+a] Liming Ying,[b] and Xue-Feng Yu*[a]

Dedication ((optional))

Abstract: The CRISPR/Cas9 system emerges as a promising tool for correcting various genetic abnormalities, and cytosolic delivery of Cas9-sgRNA (single guide RNA) ribonucleoprotein is highly desirable for therapeutic applications. Here, we report a biodegradable two-dimensional (2D) delivery platform based on loading black phosphorus nanosheets (BPs) with Cas9 ribonucleoprotein engineered with three nuclear localization signals (NLSs) at C terminus (Cas9N3). The Cas9N3-BPs enter cells effectively via membrane penetration and endocytosis pathways, followed by a BPs biodegradation-associated endosomal escape and cytosolic releases of the loaded Cas9N3 complexes. The Cas9N3-BPs thus provide efficient genome editing and gene silencing *in vitro* and *in vivo* at a relatively low dose as compared with other nanoparticles-based delivery platforms. This biodegradable 2D delivery platform offers a versatile cytosolic delivery approach for CRISPR/Cas9 ribonucleoprotein and other bioactive macromolecules for biomedical applications.

The CRISPR/Cas9 system (clustered regularly interspaced short palindromic repeat, and CRISPR-associated protein 9), originally derived from the adaptive prokaryotic immune system,[1] now has widely been applied as a prominent tool in many fields, including transcription regulation,[2] genome editing,[3] *in situ* DNA/RNA detection,[4] etc. Since the CRISPR/Cas9 system is now in fast development in aspects ranging from basic research to biomedical applications, efficient cytosolic delivery platforms of such system are highly desirable. Delivery of DNA components encoding Cas9 protein and sgRNA (single guide RNA) via viral or non-viral approaches have been reported.[5] However, therapeutic potentials of these DNA delivery approaches are limited by possible insertional mutagenesis and over-dosing, which may lead to the increased risks of genetic disorders[6] and off-target effects,[7] respectively. To overcome these problems, besides using double nicking approaches,[3b, 8] optimizing sgRNA design,[9] and engineering Cas9 for high-fidelity,[10] direct delivery of Cas9-sgRNA ribonucleoprotein complexes followed by sustained releases has been regarded as an attractive strategy.[11] Nanoparticles (NPs) have been applied as efficient cellular delivery platforms for various biomolecules, mainly due to their controllable sizes, various surface modifications, bioresponsive behaviours, as well as good loading capacities.[12] Very recently, some NPs, including DNA nanoclews,[13] Au NPs,[14] graphene oxide (GO) nanosheets,[15] and zeolitic imidazolate framework (ZIFs)[16] have been successfully employed in delivering Cas9-sgRNA complexes based on the construction of large ribonucleoprotein-NPs complexes. However, most of these NPs-based delivery platforms are non-biodegradable or degrade to products with negative long-term effects, which may impede their further therapeutic applications.

Black phosphorus nanosheets (BPs), a type of newly developed two-dimensional (2D) materials, have attracted tremendous research interests recently due to their distinctive physical and chemical properties.[17] As an allotrope of elemental phosphorus, BPs possess excellent element biocompatibility and degrade to nontoxic phosphite/phosphate ions under physiological conditions.[18] BPs with atomic thickness and a 2D puckered honeycomb structure[19] provide very high surface-to-volume ratios among various nanomaterials. Furthermore, the periodic atomic grooves on BPs' surfaces provide ideal anchoring sites for proteins[20] and other soft linear materials,[21] indicating their potentials in loading and delivery of biomolecules. Very recently, BPs-based approaches have widely been employed in numerous biomedical applications, including photothermal/photodynamic therapies,[22] biosensing,[23] and drug/biomolecules delivery.[24] However, the applications of BPs in cytosolic delivery of bioactive macromolecules have not yet been reported.

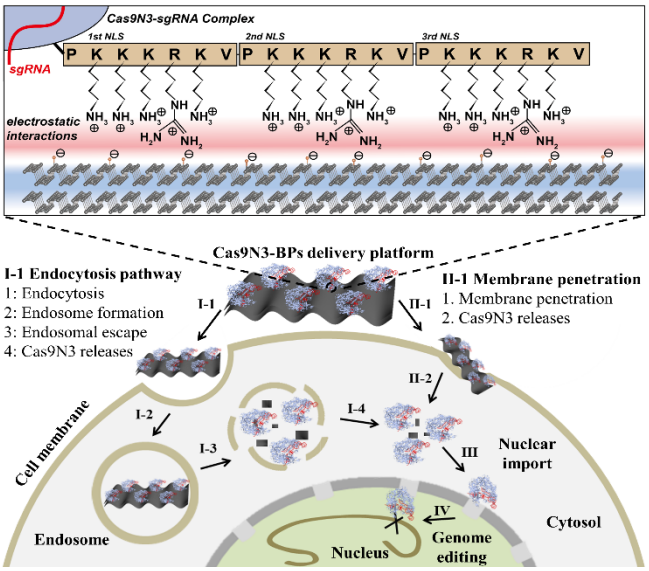

Figure 1. Design of the Cas9N3-BPs delivery platform, and its intracellular delivery via both endocytosis and direct membrane penetration pathways.

[a] Dr. W. Zhou,[+] H. Cui,[+] Prof. X.-F. Yu
Center for Biomedical Materials and Interfaces,
Shenzhen Institutes of Advanced Technology,
Chinese Academy of Sciences, Shenzhen 518055, P.R. China
E-mail: xf.yu@siat.ac.cn
[b] Dr. L. Ying
Molecular Medicine,
National Heart and Lung Institute,
Imperial College London, London SW7 2AZ, United Kingdom
[+] These authors contributed equally.

Supporting information for this article is given via a link at the end of the document.

Herein, the BPs is employed as a biodegradable 2D delivery platform for Cas9-sgRNA complexes, resulting in efficient cytosolic delivery and genome editing. As shown in Figure 1, Cas9 protein was first engineered with three repeats of nuclear localization signals (NLSs) at C terminus for the enhanced electrostatic interaction and improved nuclear targeting of the obtained Cas9-sgRNA complexes (Cas9N3). Cas9N3 ribonucleoprotein was then loaded onto the BPs via electrostatic interaction with a remarkable loading capacity of 98.7%. The constructed Cas9N3-BPs were delivered to cytoplasm via both direct membrane penetration and endocytosis pathway followed by endosomal escape upon biodegradation of the ultra-thin BPs. Cytoplasmic Cas9N3 were further imported to nuclei directed by NLSs fused to the Cas9 protein, leading to highly efficient genome editing and gene silencing *in vitro* and *in vivo*.

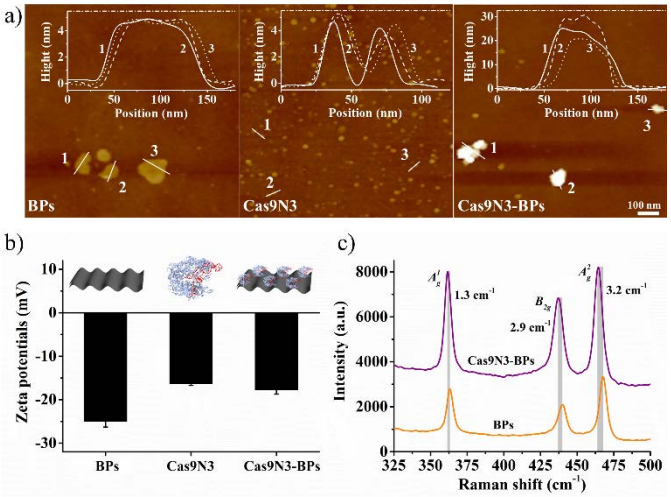

Figure 2. Characterization of Cas9N3-BPs. a) AFM images of bare BPs, free Cas9N3 and Cas9N3-BPs. The inset curves show the thicknesses measured by AFM. b) Zeta potentials of bare BPs, free Cas9N3 and Cas9N3-BPs in water. c) Raman spectra of bare BPs and Cas9N3-BPs.

Recombinant *Streptococcus pyogenes* Cas9 proteins were purified from *Escherichia coli* BL21 (DE3), and the binding/cleavage activities of Cas9-sgRNA complexes were confirmed in solution (Figure S1). The BPs were prepared by a modified liquid exfoliation method reported by our group[25] and examined by atomic force microscopy (AFM, Figure 2a) and transmission electron microscopy (TEM, Figure S2). It is observed that the BPs are ultra-thin nanosheets with an average lateral size and thickness of 100 and 4.7 nm, respectively. After loading with Cas9N3, the average thickness of the nanosheets increased to 26.4 nm, and the average zeta potential was changed from -25.1 mV of bare BPs to -17.8 mV of Cas9N3-BPs, which was close to that of Cas9N3 (-16.3 mV) (Figure 2b). Furthermore, three characteristic Raman peaks at 362, 437, and 462 cm^{-1} of BPs shift slightly after loading with Cas9N3 (Figure 2c). Variations of absorption and fluorescence in Alexa-488 labelled Cas9N3 were also found once loaded to BPs ($Cas9N3_{A488}$, Figure S3). All these results indicate the successful loading of Cas9N3 onto the BPs' surface.

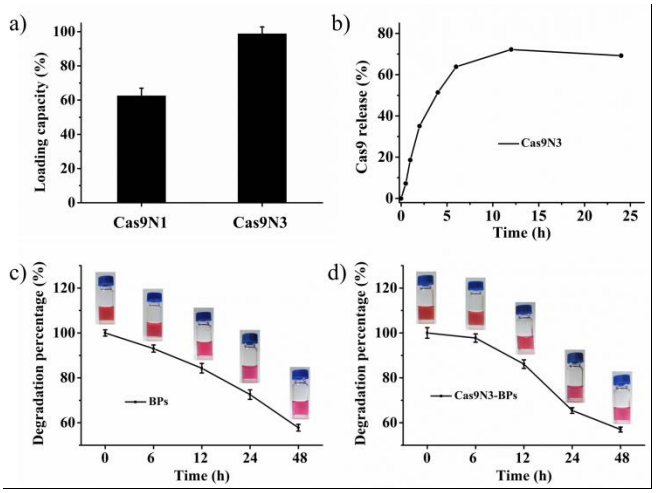

Figure 3. Cas9 loading capacity and release profile. a) Loading capacity of BPs for Cas9N1 and Cas9N3 in mass ($M_{cas9\text{-}loaded}/M_{BPs}$). b) Percentages of active Cas9N3-sgRNA complexes released from Cas9N3-BPs at different time points. Degradation of c) bare BPs and d) Cas9N3-BPs in 10% FBS DMEM at different time intervals. The insets in c) and d) show the corresponding photographs of the sample solutions.

To verify the effects of extra NLSs on the loading capacity of Cas9N3 to BPs, the Cas9 protein bearing one repeat NLS at C terminus (Cas9N1) was used as a control. A 61.7% and 73.3% decrease of active Cas9N1 and Cas9N3 in the supernatant were observed, respectively, as compared to the samples without BPs (Figure S4). It reveals 62.5% loading capacity of Cas9N1 and 98.7% of Cas9N3 in mass ($M_{Cas9\text{-}loaded}/M_{BPs}$) (Figure 3a). This is evident that the extra two repeats of NLSs dramatically enhanced electrostatic interactions between negative charged BPs and positive charged basic amino acid residues (the 12 lysine and 3 arginine residues) in NLSs of Cas9N3, resulting in a more efficient loading.

The release profile of active Cas9N3 from Cas9N3-BPs in buffer solution (10% FBS DMEM) was then investigated by monitoring the increases of active complexes in the supernatant (Figures 3b and S5). A sustained release of Cas9N3 can be observed until it reaches its maximum (72.2%) at about 12 h. The corresponding degradation of BPs with or without Cas9N3 loading was also monitored by examining the sample absorption at 808 nm. Compared with the sustained and steady degradation of bare BPs (Figure 3c), the BPs loaded with Cas9N3 show a slow degrading phase accompanying the fast releasing phase of Cas9N3 (0-12 h, Figure 3d), suggesting that the release of Cas9-sgRNA complexes was triggered by the degradation of BPs.

The cytosolic delivery performances of the Cas9N3-BPs platform were investigated by using MCF-7 cell line as a model. For fluorescence examinations, Cas9N3$_{A488}$-BPs platform was established by loading fluorescent Cas9N3$_{A488}$-sgRNA complexes onto the BPs and then applied to MCF-7 cells with a final BPs and Cas9N3$_{A488}$ concentration of 2 μg/mL and 16 nM, respectively. The intracellular delivery and localization of Cas9N3$_{A488}$ at different time points were monitored by the green fluorescence of Alexa-488 (Figures 4a and S6). The intracellular biodegradation of BPs was determined by monitoring the Raman intensity mapping with BP's characteristic A_g^1 Raman peak (Figure 4b) and average intensities of the three characteristic Raman peaks (Figure S7) in a selected cell. After 4 h of incubation, efficient internalization of Cas9N3$_{A488}$ complexes was observed around nuclei, while the intracellular Raman signals from BPs demonstrated similar distribution, indicating the integrity of internalized Cas9N3$_{A488}$-BPs platforms. At 12 h, nuclear import of Cas9N3$_{A488}$ appeared, and the Raman signals from BPs decreased significantly, suggesting the cytosolic releases of Cas9N3$_{A488}$ accompanied with the degradation of BPs. When the incubation time increased to 24 h, only faint Raman signals from BPs were observed with the nuclear import efficiency of Cas9N3$_{A488}$ increased to 78.0% (Figure 4c). Meanwhile, under the same condition, nuclear import efficiency of Cas9N1$_{A488}$ was 50.7%, clearly indicating that the presence of extra two repeats of NLSs increased the nuclear localization of Cas9 (Figures 4c and S6). As a control, free Cas9N3$_{A488}$ complexes without BPs had neglectable cytosolic delivery and nuclear import (Figures 4c and S8). These results demonstrate the efficient cytosolic delivery of active Cas9-sgRNA complexes associated with the biodegradation of BPs. Further biocompatibility assays (the MTT assay and calcein-AM/PI staining) showed that almost no cytotoxicity of Cas9N3-BPs with BPs concentration of 8 μg/mL could be found after 24 h incubation in various cell lines (Figures S9 and S10). Such biodegradable and biocompatible cellular delivery platform for Cas9-sgRNA exhibits great potentials in therapeutic applications

Since BPs-based delivery platforms had been reported to enter cells mainly through endocytic pathways,[24a, 24b] the mechanism of cellular uptake of Cas9N3$_{A488}$-BPs was investigated using different endocytosis inhibitors. Three endocytosis inhibitors, methyl-β-cyclodextrin (MβCD), sucrose, and amiloride, were employed to verify the caveolae-mediated endocytosis, clathrin-mediated endocytosis, and macropinocytosis, respectively. The endocytosis efficiency significantly decreased in cells pre-treated with MβCD and amiloride, suggesting that the endocytic uptake of Cas9N3$_{A488}$-BPs was mainly through the pathways of caveolae-dependent endocytosis and micropinocytosis (Figures 4d and S11). Interestingly, the cells pre-treated with 4 ^{o}C incubation to block all energy-dependent endocytic processes only resulted in a 69.6% decrease of intracellular intensity of Cas9N3$_{A488}$-BPs. It suggests that although endocytosis is the major cellular uptake pathway, a minor proportion of Cas9N3$_{A488}$-BPs can enter cells by a membrane penetration pathway due to their 2D morphology, as has been reported in 2D graphene sheets.[26].

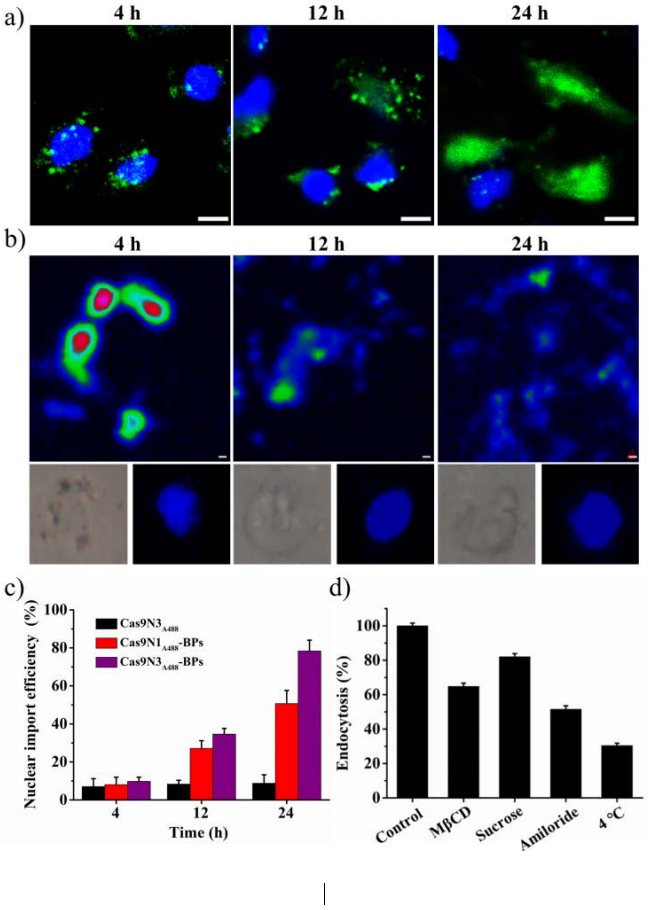

Figure 4. Intracellular delivery and degradation of Cas9N3-BPs. a) Confocal laser scanning fluorescence imaging of MCF-7 cells treated with Cas9N3$_{A488}$-BPs for different time intervals. Blue and green fluorescence images show nuclear staining with DAPI and Alexa-488, respectively. The scale indicates 50 μm. b) Intracellular degradation of BPs in a selected cell monitored by Raman intensity mapping with BP's characteristic A_g^1 Raman peak. Inset show the bright and nuclear (DAPI) image of a selected cell. The scale indicates 1.0 μm. c) Nuclear import efficiency of MCF-7 cells treated with free Cas9N3$_{A488}$, Cas9N1$_{A488}$-BPs and Cas9N3$_{A488}$-BPs at different time points. d) Inhibition of endocytosis under different inhibitors and low temperature of 4 ^{o}C.

Since the endosomal escape remains a major challenge for most NPs-based delivery platforms, the endosomal escape of Cas9N3-BPs followed by endocytosis was assessed by staining the Cas9N3$_{A488}$-BPs delivered MCF-7 cells with lysotracker dyes (Figure S12). After 4 h of incubation, most of the Cas9N3$_{A488}$ (green) colocalized with endosomes (red) giving a merged yellow colour, while isolated small green dots outside endosomes represented the membrane penetration-dependent uptake of the Cas9N3$_{A488}$-BPs. With prolonged incubation, fluorescence signals of lysotracker disappeared and Cas9N3$_{A488}$ complexes were transported to nuclei, revealing effective endosomal escape and cytosolic releases of the complexes. In addition, experiments also revealed accelerated degradation of BPs under acidic conditions in solution (Figure S13). Therefore, it can be proposed that the decrease of pH value in endosomes accelerated the degradation of BPs releasing large amounts of

phosphite/phosphate ions with elevated osmotic pressure in endosomes, which induce endosome bursts[27] and facilitate endosomal escape of loaded $Cas9N3_{A488}$ complexes.

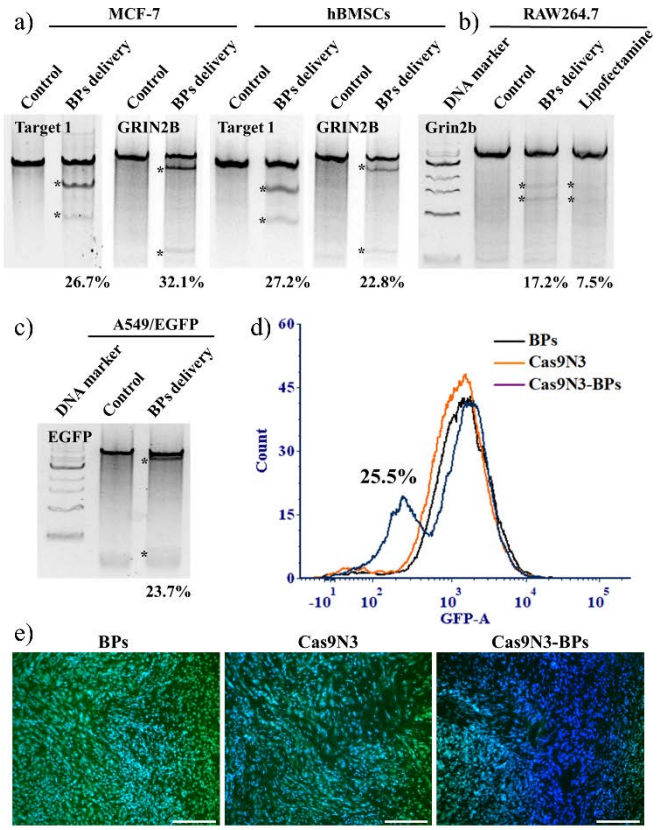

Figure 5. *In vitro* and *in vivo* genome editing and gene silencing of Cas9N3-BPs. a) Surveyor assays of MCF-7 and hBMSCs cells treated with Cas9N3-BPs. Cas9N3 were devoted to target Target 1 and GRIN2B sites of the human genome. b) Surveyor assays of RAW 264.7 cells treated with Cas9N3 via BPs delivery and Lipofectamine transfection. Cas9N3 were devoted to target Grin2b site in the mouse genome. c) Surveyor assays of A549/EGFP cells treated with Cas9N3-BPs targeting the coding region of EGFP. (Control: cells treated with only Ca9N3) d) Flow cytometry of A549/EGFP cells treated with bare BPs, free Cas9N3, or Cas9N3-BPs. e) *In vivo* delivery of Cas9N3-BPs into A549/EGFP tumor-bearing nude mice. Frozen tumor sections were collected around the site of injection on day 7 post-treatment. The scale indicates 100 μm.

Based on above evidence showing efficient nuclear transport of Cas9N3 complexes, we evaluated the capability of Cas9N3-BPs delivery platform in genome editing. Cas9N3-BPs targeting a non-coding region within the human genome, namely Target 1, was constructed and delivered to MCF-7 cells. According to ENCODE data,[28] Target 1 is within an intergenic DNase I hypersensitive site, which is relatively safe and accessible for genome editing. The cells were treated with Cas9N3-BPs for 3 days followed by genome extraction. Subsequent Surveyor assays revealed an indel frequency of 26.7% (Figure 5a). Paralleling experiments showed an indel frequency of only 15.1% of Cas9N1 complexes when delivered by BPs (Figure S14), confirming the higher loading capacity and more efficient nuclear transport of Cas9N3. Subsequently, Cas9N3-BPs targeting a site (namely GRIN2B) in gene *GRIN2B*, a gene implicated in rare neurodevelopmental disorders, was constructed and applied to MCF-7 cells, resulting in an indel frequency of 32.1% (Figure 5a). Furthermore, compared with other NPs-based delivery platforms (Table S2), the Cas9N3-BPs delivery platform can achieve comparable genome editing efficiencies at much lower concentrations of both nanoparticle (BPs) and Cas9-sgRNA complexes.

Additionally, Cas9N3-BPs targeting Target 1 and GRIN2B sites resulted in 27.2% and 22.8% indel frequencies in human bone marrow derived mesenchymal stem cells (hBMSCs, within 10 passages). To further evaluate its performances in difficult to transfect cells, Cas9N3-BPs platform targeting a homologous site in mouse *Grin2b* gene (namely Grin2b) was applied to RAW 264.7 cells line. As shown in Figure 5b, although the genome editing efficiency of Cas9N3-BPs (17.2%) is relatively low in RAW 264.7 cells as compared with those observed in other cells, it still outperforms Lipofectamine-mediated transfection, whose efficiency is only 7.5%.

We also evaluated the capability of Cas9N3-BPs delivery platform in gene silencing, with a sgRNA targeting the coding region of enhanced green fluorescent protein (EGFP) in A549 cells stably expressing EGFP (A549/EGFP). Five days after initial treatment with Cas9N3-BPs, decreased EGFP fluorescence was observed (Figure S15), suggesting successful cleavages of EGFP coding region and shifts of the reading frame. Surveyor assay and quantitative flow cytometry analysis revealed an indel frequency of 23.7%, and an EGFP silencing efficiency of 25.5% in cells treated with Cas9N3-BPs, while free Cas9N3 complexes had neglectable effects. (Figures 5c, 5d and S15).

The *in vivo* therapeutic potentials of the Cas9N3-BPs platform were also evaluated using A549/EGFP tumor-bearing nude mice as models. As shown in Figures 5e and S16, 7 days after intratumoral injection of Cas9N3-BPs targeting the coding region of EGFP, significant reduction of EGFP signals were observed in the frozen tumor sections around the site of injection, while tumors treated with BPs or free Cas9N3 did not show any reduction of EGFP signals.

In conclusion, a biodegradable 2D BPs-based CRISPR/Cas9 ribonucleoprotein delivery system has been successfully established for efficient genome editing and gene silencing. A Cas9 protein with three NLSs at C terminus is engineered to strengthen its electrostatic interaction with BPs, resulting in improved loading capacity of 98.7% and enhanced nuclear transport efficiency. The Cas9N3-BPs delivery platform can effectively enter cells via membrane penetration and endocytosis pathways, which is followed by a BPs biodegradation-associated endosomal escape and cytosolic releases of the loaded Cas9N3 complexes. Furthermore, *in vitro* and *in vivo* studies both demonstrate that the constructed Cas9N3-BPs platforms resulted in efficient genome editing and gene silencing at a relatively low dose as compared with other NPs-based delivery platforms. This simple and versatile cytosolic delivery approach may extend to other bioactive macromolecules for biomedical applications, and its superior biocompatibility and

biodegradability may open new avenues in gene therapy and personalized medicine.

Acknowledgements

This work was jointly supported by the National Natural Science Foundation of China (31600595 and 51672305), International Cooperation Project for Science and Research Plan of Shenzhen (GJHZ20160229195805334), Frontier Science Key Programs of Chinese Academy of Sciences (QYZDB-SSW-SLH034), and the Leverhulme Trust (RPG-2015-345 to L.Y.).

Keywords: black phosphorus • CRISPR/Cas9 • two-dimensional materials • genome editing • gene silencing

[1] P. Horvath, R. Barrangou, *Science* **2010**, *327*, 167-170.
[2] a) P. Mali, J. Aach, P. B. Stranges, K. M. Esvelt, M. Moosburner, S. Kosuri, L. Yang, G. M. Church, *Nat. Biotechnol.* **2013**, *31*, 833-838; b) S. Konermann, M. D. Brigham, A. E. Trevino, J. Joung, O. O. Abudayyeh, C. Barcena, P. D. Hsu, N. Habib, J. S. Gootenberg, H. Nishimasu, O. Nureki, F. Zhang, *Nature* **2015**, *517*, 583-588.
[3] a) J. A. Doudna, E. Charpentier, *Science* **2014**, *346*, 1258096; b) S. Q. Tsai, N. Wyvekens, C. Khayter, J. A. Foden, V. Thapar, D. Reyon, M. J. Goodwin, M. J. Aryee, J. K. Joung, *Nat. Biotechnol.* **2014**, *32*, 569-576.
[4] a) W. Deng, X. Shi, R. Tjian, T. Lionnet, R. H. Singer, *Proc. Natl. Acad. Sci. U. S. A.* **2015**, *112*, 11870-11875; b) D. A. Nelles, M. Y. Fang, M. R. O'Connell, J. L. Xu, S. J. Markmiller, J. A. Doudna, G. W. Yeo, *Cell* **2016**, *165*, 488-496.
[5] a) R. Cheng, J. Peng, Y. Yan, P. Cao, J. Wang, C. Qiu, L. Tang, D. Liu, L. Tang, J. Jin, X. Huang, F. He, P. Zhang, *FEBS. Lett.* **2014**, *588*, 3954-3958; b) M. Tabebordbar, K. Zhu, J. K. W. Cheng, W. L. Chew, J. J. Widrick, W. X. Yan, C. Maesner, E. Y. Wu, R. Xiao, F. A. Ran, L. Cong, F. Zhang, L. H. Vandenberghe, G. M. Church, A. J. Wagers, *Science* **2016**, *351*, 407-411; c) H. Yin, W. Xue, S. Chen, R. L. Bogorad, E. Benedetti, M. Grompe, V. Kotelianský, P. A. Sharp, T. Jacks, D. G. Anderson, *Nat. Biotechnol.* **2014**, *32*, 551-553; d) P. Wang, L. Zhang, W. Zheng, L. Cong, Z. Guo, Y. Xie, L. Wang, R. Tang, Q. Feng, Y. Hamada, K. Gonda, Z. Hu, X. Wu, X. Jiang, *Angew. Chem. Int. Ed. Engl.* **2018**, *57*, 1491-1496.
[6] S. Hacein-Bey-Abina, A. Garrigue, G. P. Wang, J. Soulier, A. Lim, E. Morillon, E. Clappier, L. Caccavelli, E. Delabesse, K. Beldjord, V. Asnafi, E. MacIntyre, L. Dal Cortivo, I. Radford, N. Brousse, F. Sigaux, D. Moshous, J. Hauer, A. Borkhardt, B. H. Belohradsky, U. Wintergerst, M. C. Velez, L. Leiva, R. Sorensen, N. Wulffraat, S. Blanche, F. D. Bushman, A. Fischer, M. Cavazzana-Calvo, *J. Clin. Invest.* **2008**, *118*, 3132-3142.
[7] Y. Fu, J. A. Foden, C. Khayter, M. L. Maeder, D. Reyon, J. K. Joung, J. D. Sander, *Nat. Biotechnol.* **2013**, *31*, 822-826.
[8] F. A. Ran, P. D. Hsu, C. Y. Lin, J. S. Gootenberg, S. Konermann, A. E. Trevino, D. A. Scott, A. Inoue, S. Matoba, Y. Zhang, F. Zhang, *Cell* **2013**, *154*, 1380-1389.
[9] J. G. Doench, N. Fusi, M. Sullender, M. Hegde, E. W. Vaimberg, K. F. Donovan, I. Smith, Z. Tothova, C. Wilen, R. Orchard, H. W. Virgin, J. Listgarten, D. E. Root, *Nat. Biotechnol.* **2016**, *34*, 184-191.
[10] a) B. P. Kleinstiver, V. Pattanayak, M. S. Prew, S. Q. Tsai, N. T. Nguyen, Z. Zheng, J. K. Joung, *Nature* **2016**, *529*, 490-495; b) I. M. Slaymaker, L. Gao, B. Zetsche, D. A. Scott, W. X. Yan, F. Zhang, *Science* **2016**, *351*, 84-88; c) P. I. Kulcsar, A. Talas, K. Huszar, Z. Ligeti, E. Toth, N. Weinhardt, E. Fodor, E. Welker, *Genome. Biol.* **2017**, *18*, 190.
[11] W. J. Sun, Z. Gu, *Sci. China. Mater.* **2017**, *60*, 511-515.
[12] a) L. Y. Chou, K. Ming, W. C. Chan, *Chem. Soc. Rev.* **2011**, *40*, 233-245; b) V. Biju, *Chem. Soc. Rev.* **2014**, *43*, 744-764; c) S. Zhang, H. Gao, G. Bao, *ACS Nano* **2015**, *9*, 8655-8671; d) Y. Lu, A. A. Aimetti, R. Langer, Z. Gu, *Nat. Rev. Mater.* **2017**, *2*, *16075*.
[13] W. Sun, W. Ji, J. M. Hall, Q. Hu, C. Wang, C. L. Beisel, Z. Gu, *Angew. Chem. Int. Ed. Engl.* **2015**, *54*, 12029-12033.
[14] a) R. Mout, M. Ray, G. Yesilbag Tonga, Y. W. Lee, T. Tay, K. Sasaki, V. M. Rotello, *ACS Nano* **2017**, *11*, 2452-2458; b) K. Lee, M. Conboy, H. M. Park, F. Jiang, H. J. Kim, M. A. Dewitt, V. A. Mackley, K. Chang, A. Rao, C. Skinner, T. Shobha, M. Mehdipour, H. Liu, W. C. Huang, F. Lan, N. L. Bray, S. Li, J. E. Corn, K. Kataoka, J. A. Doudna, I. Conboy, N. Murthy, *Nat. Biomed. Eng.* **2017**, *1*, 889-901.
[15] H. Yue, X. Zhou, M. Cheng, D. Xing, *Nanoscale* **2018**, *10*, 1063-1071.
[16] S. K. Alsaiari, S. Patil, M. Alyami, K. O. Alamoudi, F. A. Aleisa, J. S. Merzaban, M. Li, N. M. Khashab, *J. Am. Chem. Soc.* **2018**, *140*, 143-146.
[17] a) W. Lei, G. Liu, J. Zhang, M. Liu, *Chem Soc Rev* **2017**, *46*, 3492-3509; b) Y. Yi, X.-F. Yu, W. Zhou, J. Wang, P. K. Chu, *Mater. Sci. Eng. R: Rep.* **2017**, *120*, 1-33.
[18] Q. Zhou, Q. Chen, Y. Tong, J. Wang, *Angew. Chem. Int. Ed. Engl.* **2016**, *55*, 11437-11441.
[19] A. Castellanos-Gomez, *J. Phys. Chem. Lett.* **2015**, *6*, 4280-4291.
[20] W. Zhang, T. Huynh, P. Xiu, B. Zhou, C. Ye, B. Q. Luan, R. H. Zhou, *Carbon* **2015**, *94*, 895-902.
[21] D. W. Kim, H. S. Jeong, K. O. Kwon, J. M. Ok, S. M. Kim, H. T. Jung, *Adv. Mater. Interfaces.* **2016**, *3*. 22
[22] a) Z. B. Sun, H. H. Xie, S. Y. Tang, X. F. Yu, Z. N. Guo, J. D. Shao, H. Zhang, H. Huang, H. Y. Wang, P. K. Chu, *Angew. Chem. Int. Edit.* **2015**, *54*, 11526-11530; b) J. Shao, H. Xie, H. Huang, Z. Li, Z. Sun, Y. Xu, Q. Xiao, X. F. Yu, Y. Zhao, H. Zhang, H. Wang, P. K. Chu, *Nat. Commun.* **2016**, *7*, 12967.
[23] Y. T. Chen, R. Ren, H. H. Pu, J. B. Chang, S. Mao, J. H. Chen, *Biosens. Bioelectron.* **2017**, *89*, 505-510.
[24] a) W. Tao, X. B. Zhu, X. H. Yu, X. W. Zeng, Q. L. Xiao, X. D. Zhang, X. Y. Ji, X. S. Wang, J. J. Shi, H. Zhang, L. Mei, *Adv. Mater.* **2017**, *29*; b) W. S. Chen, J. Ouyang, H. Liu, M. Chen, K. Zeng, J. P. Sheng, Z. J. Liu, Y. J. Han, L. Q. Wang, J. Li, L. Deng, Y. N. Liu, S. J. Guo, *Adv. Mater.* **2017**, *29*; c) H. Wang, L. Zhong, Y. Liu, X. Xu, C. Xing, M. Wang, S. M. Bai, C. H. Lu, H. H. Yang, *Chem. Commun. (Camb)* **2018**, *54*, 3142-3145.
[25] Z. Guo, H. Zhang, S. Lu, Z. Wang, S. Tang, J. Shao, Z. Sun, H. Xie, H. Wang, X.-F. Yu, P. K. Chu, *Adv. Funct. Mater.* **2015**, *25*, 6996–7002.
[26] Y. F. Li, H. Y. Yuan, A. von dem Bussche, M. Creighton, R. H. Hurt, A. B. Kane, H. J. Gao, *Proc. Natl. Acad. Sci. U. S. A.* **2013**, *110*, 12295-12300.
[27] J. Li, Y. C. Chen, Y. C. Tseng, S. Mozumdar, L. Huang, *J. Control. Release* **2010**, *142*, 416-421.
[28] I. Dunham, A. Kundaje, S. F. Aldred, P. J. Collins, C. Davis, F. Doyle, C. B. Epstein, S. Frietze, J. Harrow, R. Kaul, J. Khatun, B. R. Lajoie, S. G. Landt, B. K. Lee, F. Pauli, K. R. Rosenbloom, P. Sabo, A. Safi, A. Sanyal, N. Shoresh, J. M. Simon, L. Song, N. D. Trinklein, R. C. Altshuler, E. Birney, J. B. Brown, C. Cheng, S. Djebali, X. J. Dong, I. Dunham, J. Ernst, T. S. Furey, M. Gerstein, B. Giardine, M. Greven, R. C. Hardison, R. S. Harris, J. Herrero, M. M. Hoffman, S. Iyer, M. Kellis, J. Khatun, P. Kheradpour, A. Kundaje, T. Lassmann, Q. H. Li, X. Lin, G. K. Marinov, A. Merkel, A. Mortazavi, S. C. J. Parker, T. E. Reddy, J. Rozowsky, F. Schlesinger, R. E. Thurman, J. Wang, L. D. Ward, T. W. Whitfield, S. P. Wilder, W. Wu, H. L. S. Xi, K. Y. Yip, J. L. Zhuang, B. E. Bernstein, E. Birney, I. Dunham, E. D. Green, C. Gunter, M. Snyder, M. J. Pazin, R. F. Lowdon, L. A. L. Dillon, L. B. Adams, C. J. Kelly, J. Zhang, J. R. Wexler, E. D. Green, P. J. Good, E. A. Feingold, B. E. Bernstein, E. Birney, G. E. Crawford, J. Dekker, L. Elnitski, P. J. Farnham, M. Gerstein, M. C. Giddings, T. R. Gingeras, E. D. Green, R. Guigo, R. C. Hardison, T. J. Hubbard, M. Kellis, W. J. Kent, J. D. Lieb, E. H. Margulies, R. M. Myers, M. Snyder, J. A. Stamatoyannopoulos, S. A. Tenenbaum, et al., *Nature* **2012**, *489*, 57-74.

Entry for the Table of Contents

COMMUNICATION

A biodegradable two-dimensional delivery platform for CRISPR/Cas9 is successfully established based on loading black phosphorus nanosheets with engineered Cas9 ribonucleoprotein, enabling controlled cytosolic release and genome editing with high efficiency.

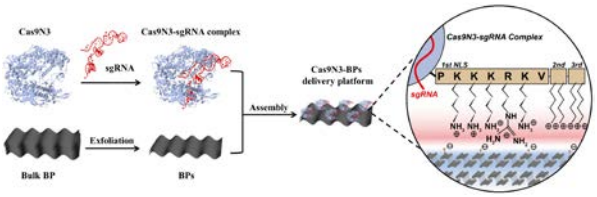

*Wenhua Zhou, Haodong Cui, Liming Ying, and Xue-Feng Yu**

Page No. – Page No.

Enhanced Cytosolic Delivery and Releases of CRISPR/Cas9 by Black Phosphorus Nanosheets for Genome Editing